Evaluation of Turbulence Modelsfor Flow with Shock Waves in a Transonic Diffuser

San L. Tolentino
Research collaborator
Group of Mathematical Modeling and Numerical Simulation (GMMNS)
Universidad Nacional de Ingeniería (UNI)
Lima
Perú
Universidad Nacional Experimental Politécnica "AJS"(UNEXPO)
Bolívar
Venezuela

Jorge Mírez
Elec. Mech, Eng.; MSc & Dr Physics
Professor
Group of Mathematical Modeling and Numerical Simulation (GMMNS)
Faculty of Oil, Natural Gas and Petrochemical Engineering
Universidad Nacional de Ingeniería (UNI)
Lima
Perú

In this work, five turbulence models (k-epsilon, k-omega, SST k-omega, SA, and SAS) are evaluated for turbulent flow in a transonic diffuser used in experimental tests to generate shock waves. The models were employed within the RANS framework. Transient simulations were performed in two-dimensional computational domains for pressure ratios r_p = 0.82 and r_p = 0.72 using ANSYS Fluent R16.2. Sutherland's law was applied for temperature-dependent viscosity. The results were compared with expe–rimental data for pressure, velocity, and Mach number. For pressure, the SAS model yielded a global average error of 2.62%. In the flow separation region on the upper wall of the diffuser (at the extremities of the shock front), all five models showed significant deviations from the experimental velocity data in certain regions. Regarding the Mach number, the models predicted different shock-front positions. For the maximum Mach number at the shock front, the SAS model produced errors of0.162% (r_p = 0.82) and 11.821% (r_p = 0.72), respectively.

Keywords: *Shock waves, Turbulence model, Transient simulation, Transonic Diffuser*

1. INTRODUCTION

Computational simulations in the field of fluid mec–hanics require turbulence models to be coupled with the Reynolds-Averaged Navier-Stokes (RANS) equations [1,2]. Turbulence models are semi-empirical equations that attempt to emulate the behavior of flow turbulence; however, not all of them meet the requirement of having a good representation of the compressible flow regime behavior in the regions before and after the shock front. Likewise, they present different performance levels for compressible and incompressible flow applications. When turbulent flow is simulated in computational do–mains, pressure, temperature, density, velocity, and ot–her thermodynamic parameter gradients are present [1,2].

In the flow regions adjacent to the walls, boundary layer separation, flow recirculation, free shock sepa–ration (FSS), restricted shock separation (RSS), back–pressure, and lateral pressure loads occur [2,3]. Furt–hermore, in the central flow region, where the flow decelerates due to the presence of the normal shock wave, this abrupt change in flow velocity affects its ends with the generation of oblique shock waves, where the turbulent boundary layer interacts with the shock wave, causing instability in the shock wave position [2,3]. Furthermore, flow separation modes extend to different geometries in the compressible-flow domain [3,4].

Turbulence models applied to Computational Fluid Dynamics (CFD) in a steady or transient state have different behaviors regarding the pressure, velocity, temperature, Mach number, and other thermodynamic parameter fields [1,2,5]. For the mathematical model and flow simulation, different solution mechanisms are employed, among them Direct Numerical Simulations (DNS) which do not employ turbulence models. Likewise, there are models for Large-Eddy Simulation (LES) and Detached-Eddy Simulation (DES) [1], [5].

In the field of fluid mechanics for compressible flow, tests are frequently carried out with experimental equipment of different geometries, with the purpose of capturing images of flow turbulence with the presence of shock waves [6-9].

Several authors have conducted research and simu–lated flows using various turbulence models, comparing their results with experimental data for geometries such as supersonic nozzles [10-13]; diffusers [14-18]; Ven–turi tubes [19-22]; ejectors [23-25], ducts [26-28], and other experimental equipment [29]. Where turbulence models are limited in certain regions in their ability to follow the trends observed in experimental data.

In the literature, works have been reported on transonic diffusers used as experimental equipment that generate shock waves, and one of them is the Sajben transonic diffuser [30], which is of interest in the present study. The compressible flow in the Sajben ex–perimental equipment is subjected to different pressure ratios, with the purpose of studying flow fluctuations and the presence of shock waves [30]. The diffuser geo–metry is asymmetric, with the lower part being flat and the upper part convergent-divergent, and the narrowest part is curved, which is the throat section. For this reason, due to the geometric conditions of the diffuser wall profiles, the shock wave structure is induced to its characteristic formation in response to pressure changes. Some of the most relevant works are mentioned below.

Sajben and Kroutil [30] carried out flow studies on the initial effect of the turbulent boundary layer. Salmon et al. [31] performed studies for flow with pressure

Received: July 2026, Accepted: August 2026
Correspondence to: Dr. Jorge Mírez, Faculty of Oil, Natural Gas and Petrochemical Engineering
Universidad Nacional de Ingeniería (UNI), Lima, Perú
E-mail: jmirez@uni.edu.pe
doi: 10.5937/fme2604612T
© Faculty of Mechanical Engineering, Belgrade. Allrights reserved

ratios of r_p = 0.82 and r_p = 0.72, and carried out measurements with a laser Doppler velocimeter to record flow fluctuations and oscillations. Bogar et al. [32] addressed the study of the frequency characteristics of flow oscillations. Georgiadis et al. [17] conducted evaluations of turbulence models for pressure ratios of r_p = 0.82 and r_p = 0.72, which were compared with experimental pressure and velocity data; the flow was simulated with the PARC code.Hosder et al. [33] performed studies on grid density evaluating different turbulence models for flow pressure ratios of r_p = 0.82 and r_p = 0.72; the flow was simulated with the GASP code. Tolentino [15] evaluated turbulence models for pressure ratios of r_p = 0.82 and r_p = 0.72; the flow was simulated in steady state with the ANSYS-Fluent code.

Based on the study interest of previous works, the objective of the present work is to evaluate of five turbulence models for transient flow conditions; thus, determining which of them is the most suitable for practical applications. The results of the numerical simulation curves are compared with experimental data reported in the literature. The five turbulence models to be employed are the k-epsilon model by Launder and Spalding [34], k-omega model by Wilcox [35], SST k-omega model by Menter [36], SA model by Spalart and Allmaras [37], and finally the Scale Adaptive Simulation (SAS) turbulence model by Menter and Egorov [38]. These mentioned turbulence models, among others, are part of the selection library for modeling flow behavior in various CFD codes. Therefore, it is not necessary to incorporate them manually into the code to be used. Section 2 presents the methodology. Section 3 presents the results. Finally, Section 4 presents the conclusions of the analysis carried out.

2. MATERIALS AND METHODS

The experimental equipment under study is a transonic diffuser that has been used by Sajben et al. [30] in multiple experimental tests. In the present work, only two pressure ratio cases are addressed: r_p = 0.82 for a shock wave with Mach 1.235 and r_p = 0.72 for a shock wave with Mach 1.353 [31]. For this purpose, five turbulence models are evaluated for transient air flow using the ANSYS-Fluent R16.2 code, which applies the Finite Volume Method (FVM) [5].

2.1 Mathematical Fundamentals

For the numerical solution of the compressible flow field in 2D under transient conditions, the RANS model was employed.

The governing equations are expressed as the continuity (1), momentum (2), energy (3), and the ideal gas equation of state (4) [39]:

$$\frac{\partial \rho}{\partial t} + \nabla \cdot \left(\rho u_i \right) = 0 \tag{1}$$

$$\frac{\partial \left(\rho u_i \right)}{\partial t} + \nabla \cdot \left(\rho u_i u_j \right) = -\nabla p + \nabla \cdot \left(\bar{\bar{\tau}} \right) + \nabla \cdot \left(-\overline{\rho u_i' u_j'} \right) \tag{2}$$

$$\frac{\partial \left(\rho E \right)}{\partial t} + \nabla \cdot \left(u_i \left(\rho E + p \right) \right) = \nabla \cdot \left(k_{eff} \nabla T + \left(\bar{\bar{\tau}}_{eff} \cdot u_i \right) \right) \tag{3}$$

$$p = \rho R T \tag{4}$$

where ρ is the density, u is the velocity, t is the time, p is the pressure, $\bar{\bar{\tau}}$ is the stress tensor, and the Reynolds stress term is expressed as $u_i' u_j'$. E is the total energy, T is the temperature, k_{eff} is the effective thermal conductivity, and $\bar{\bar{\tau}}_{eff}$ is the effective stress tensor. Likewise, R is the gas constant.

The air parameters are the specific heat ratio γ = 1.4, the specific heat at constant pressure c_p = 1006.43 J/(kg·K), the thermal conductivity k^t = 0.0242 W/(m·K), and the gas constant R = 287 J/(kg·K) [39]. For the viscosity as a function of temperature, the Sutherland equation [40] was used.

Five turbulence models were employed to be evaluated and compared with experimental pressure and velocity data for the air flow in a transonic diffuser [17]. The five turbulence models are presented in Table 1.

Table 1.Turbulence models used in the flow simulation

Model	Reference
k-epsilon	[34]
k-omega	[35]
SST k-omega	[36]
SA	[37]
SAS	[38]

2.2 Computationaldomain and mesh

The geometry of the computational domain of the transonic diffuser is shown in Fig. 1(a), with the lower part being planar and the upper part curved, which leads to the convergent-divergent geometry, the narrowest part being the throat section. The geometric dimensions are reported in [30,31]. Along the x-axis, at the throat section of the diffuser, h_0 = 44 mm; from this reference toward the left end, the length is -4.04h_0, and toward the right end, the length is 8.65h_c. This length along the x-axis was defined as h_x = 8.65h_0. The convergent section lies in the range from x/h_x = -0,46 to x/h_x = 0, and the divergent section in the range from x/h_x = -0 to x/h_x = 1.

Fig. 1(b) shows the meshed domain with structured quadrilateral cells, which corresponds to mesh 3, and this mesh 3 was selected after a mesh sensitivity analysis study.

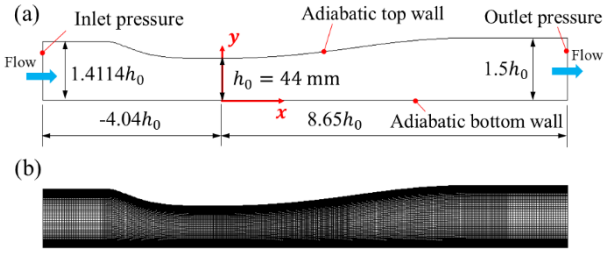


Figure1.(a) 2D computational domain for the transonic diffuser geometry. (b) Meshed domain with structured quadrilateral cells: Mesh 3 with 46970 elements

Table 2 presents the inlet and outlet values of pressure and temperature for the two pressure ratio cases, r_p = 0.82 and r_p = 0.72; where rp = $P_{outlet}/P_{0,inlet}$. The diffuser walls were considered adiabatic. The velocity at a solid wall is zero due to the no-slip

condition. It should be noted that, for these two pressure ratio conditions, the flow exhibits a transonic regime for the diffuser geometry.

Table 2. Pressure and temperature data [17]

r_p	Inlet: P_0 [Pa]	Outlet: P [Pa]	Temp.: T_0 [K]
0.82	135004.1	110664.8	300
0.72	135004.1	97219.5	300

2.3 Numerical convergence analysis

A mesh sensitivity study was carried out for the case ofthree 2D meshed domains: Mesh 1, Mesh 2, and Mesh 3; of these, Mesh 1 and Mesh 2 are not shown in Fig. 1. The meshing for the three domains was performed on the ANSYS-Meshing platform using ICEM-CFD inte–raction. Fig. 2 illustrates the behavior of y^+ in terms of the shear stress value, for the case of the pressure ratio r_p, where the y^+ values are higher in the convergent section of the diffuser and lower in the divergent section.

Mesh 2 and Mesh 3 presented better responses, since both domains had the mesh refined toward the adiabatic walls due to the presence of shear stresses. Although Mesh 3 is more refined toward the walls, it exhibits the same y^+ behavior as Mesh 2. The domains for Meshes 1, 2, and 3 were evaluated with the SAS turbulence model [38] in transient state, since this model presented better results compared to the other models presented in Table 1.

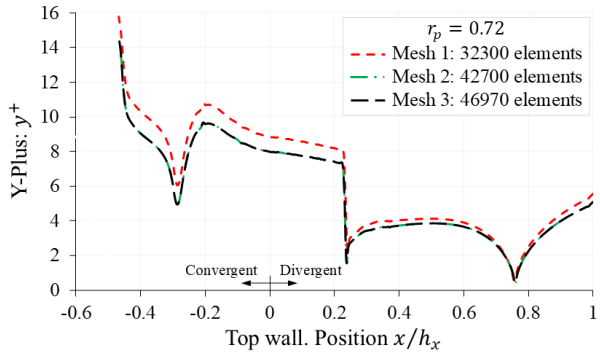


Figure 2. y^+ behavior for the meshed domain: Mesh 1, Mesh 2, and Mesh 3

2.4 Computational solution method

A density-based solver was used for two-dimensional transient flow with an implicit formulation. For flow: second-order upwind; initialization methods: hybrid; residual monitor: 1×10^{-6}. The computational simulations for the five turbulence models covered a range of 21300 to 99450 iterations.

A computer equipment with the following charac–teristics was used: CPU Dell, Optiplex 7010 model, i5, 32 GB RAM.

3. RESULTS AND DISCUSSION

In this section, the numerical results are presented, wh–ich are compared with experimental data for pressure [17,30], velocity [17], and Mach number [31].

3.1 Flow pressure

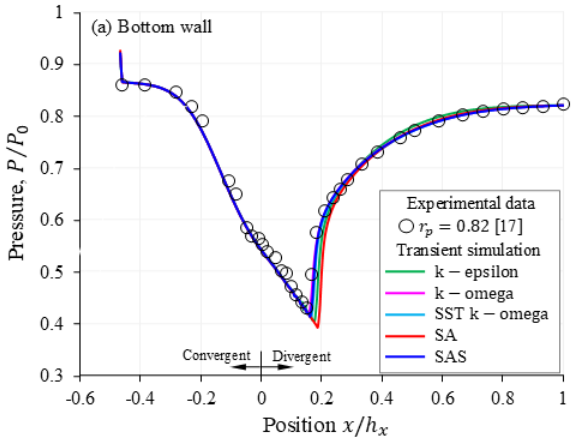
The behavior of the pressure profiles on the adiabatic walls of the transonic diffuser, for the five turbulence models and experimental pressure data for the pressure ratio r_p = 0.82, is illustrated in Fig. 3. Fig. 3(a) corres–ponds to the lower wall and Fig. 3(b) corresponds to the upper wall. The pressure drops approach up to the esti–mated position x/h_x = 0.18, and after the shock the pressure increases up to the diffuser outlet.

The curves of the five turbulence models for the developed flow exhibit the same behavior during the pressure drop, being close to and superimposed on the experimental pressure data. However, after the shock, the boundary layer separation causes the numerical curves to deviate from the experimental data up to the estimated position x/h_x = 0.38, and then downstream of this position the curves are once again close to and superimposed on the experimental data. In the estimated stretch from x/h_x = 0.18 to x/h_x = 0.38, the k-omega and SAS turbulence models are more closely fitted to the experimental pressure data, while the SA, k-epsilon, and SST k-omega models are farther away.

The effect of the boundary layer separation on the turbulence models is evident, due to their design architecture in attempting to emulate the behavior of the pressure increase after the presence of the shock wave. Table 3 presents the average percentage relative errors for the pressure ratio r_p = 0.82.

Meanwhile, Fig. 4 presents the behavior of the turbulence model curves and the experimental data for the pressure ratio r_p = 0.72. Fig. 4(a) corresponds to the lower wall and Fig. 4(b) corresponds to the upper wall. The curves that are farther apart in the estimated stretch from /h_x = 0.2 to x/h_x = 0.7 are those for the k-epsilon and k-omega turbulence models, and those that are more closely fitted to the experimental data are for SAS, SST k-omega, and SA. It is observed that there is a strong boundary layer separation for the k-omega turbulence model before the shock and for k-epsilon after the shock. Table 4 presents the average percentage relative error values for the pressure ratio r_p = 0.72.

Other turbulence models reported in previous stu–dies [15,17,41] presented similar results regarding the lateral pressure loads on the diffuser walls, which vali–dates the trend observed in the present work. Therefore, the pressure curves reveal the sensitivity of turbulence models to the adverse pressure gradient imposed by the normal shock wave, this being one of the most chal–lenging regions for numerical modeling. In the region upstream of the shock wave, all models adequately predict the pressure drop, indicating that conventional RANS model architectures are capable of reproducing transonic flow when it remains attached to the wall, without significant disturbances. However, the inter–action of the shock wave with the boundary layer causes its separation, generating a recirculation zone and strong pressure gradients. It is precisely in this separation zone where the most notable differences among turbulence models become evident, reflecting the inherent limita–tions of their formulations to capture such complex phenomena.



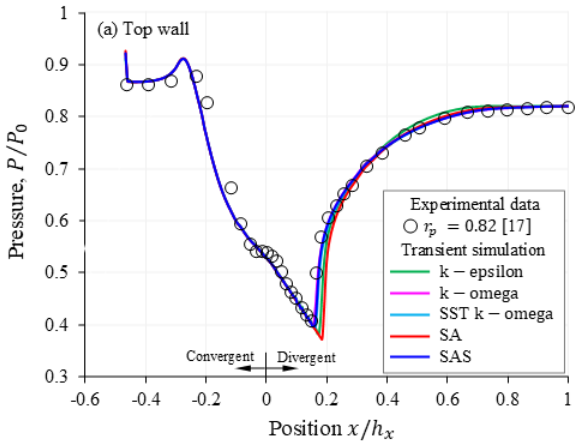
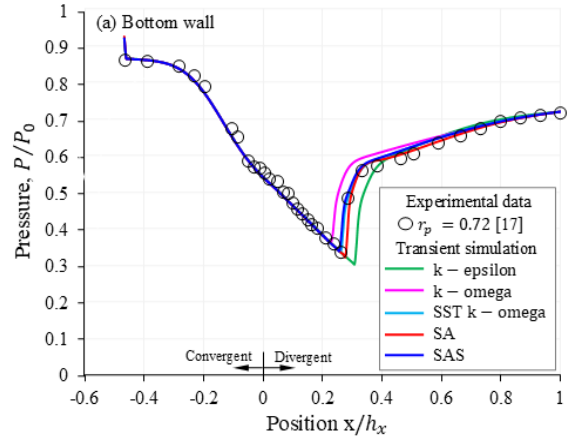


Figure 3. Comparison of curves from five turbulence models with experimental pressure data for r_p = 0.82 [17]



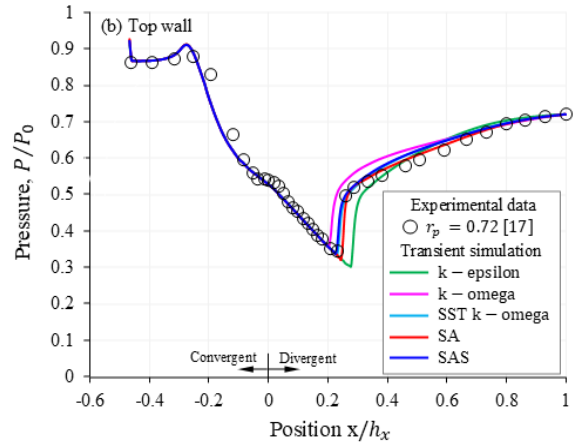


Figure 4. Comparison of curves from five turbulence models with experimental pressure data for r_p = 0.72 [17]

Table3. Average percentage relative errors of five turbulence models with respect to experimental pressure data for r_p = 0.82

Model	Bottom wall	Top wall
k-epsilon	5.52%	6.17%
k-omega	2.37%	2.02%
SST k-omega	3.86%	3.62%
SA	8.69%	8.89%
SAS	3.96%	2.84%

Table 4. Average percentage relative errors of five turbulence models with respect to experimental pressure data for r_p = 0.72

Model	Bottom wall	Top wall
k-epsilon	9.49%	12.48%
k-omega	7.90%	3.04%
SST k-omega	0.71%	3.27%
SA	3.67%	7.26%
SAS	1.39%	2.31%

To select which turbulence model best fits the experimental pressure data, the overall average of the percentage relative errors was obtained, which showed that the SAS model presents the lowest percentage relative error of 2.62%, followed by the SST k-omega turbulence model with 2.87%. Meanwhile, k-epsilon presents the highest percentage relative error of 8.42%.

Based on the results for the pressure case, the choice of the turbulence model is significant and relevant, since an inadequate turbulence model for the flow regime conditions in a computational domain presents results that are far from reality, which leads to false expectations in the predictions of shock front simulations and for the flow regions adjacent to the walls of the computational domain under study.

Table 5. Global average percentage relative error

Model	Globalaverage
k-epsilon	8.42%
k-omega	3.83%
SST k-omega	2.87%
SA	7.13%
SAS	2.62%

3.2 Flow velocity

The velocity profiles for r_p = 0.82 (Fig. 5) and r_p = 0.72 (Fig. 6) have been evaluated at four positions upstream of the shock front, at the positions x/h_0 = 2.882, (x/h_x = 0.333), x/h_0 = 4.611, (x/h_x = 0.533), x/h_0 = 6.34, (x/h_x = 0.732) and x/h_0 = 7.493, (x/h_x = 0.866), where the curves of the five turbulence models are superimposed in certain stretches and fluctuate around the experimental velocity data in other stretches.

It is observed that for r_p = 0.82 and r_p = 0.72, the SAS turbulence model, compared to k-omega, presents a better approximation to the experimental velocity data in the central region of the flow and in the lower part of the diffuser wall. However, in the upper region of the diffuser, the five turbulence model curves are separated from the experimental velocity data, and this wall region, which has convergent and divergent curvature, has a significant effect in the divergent section after flow separation, where flow recirculation occurs.

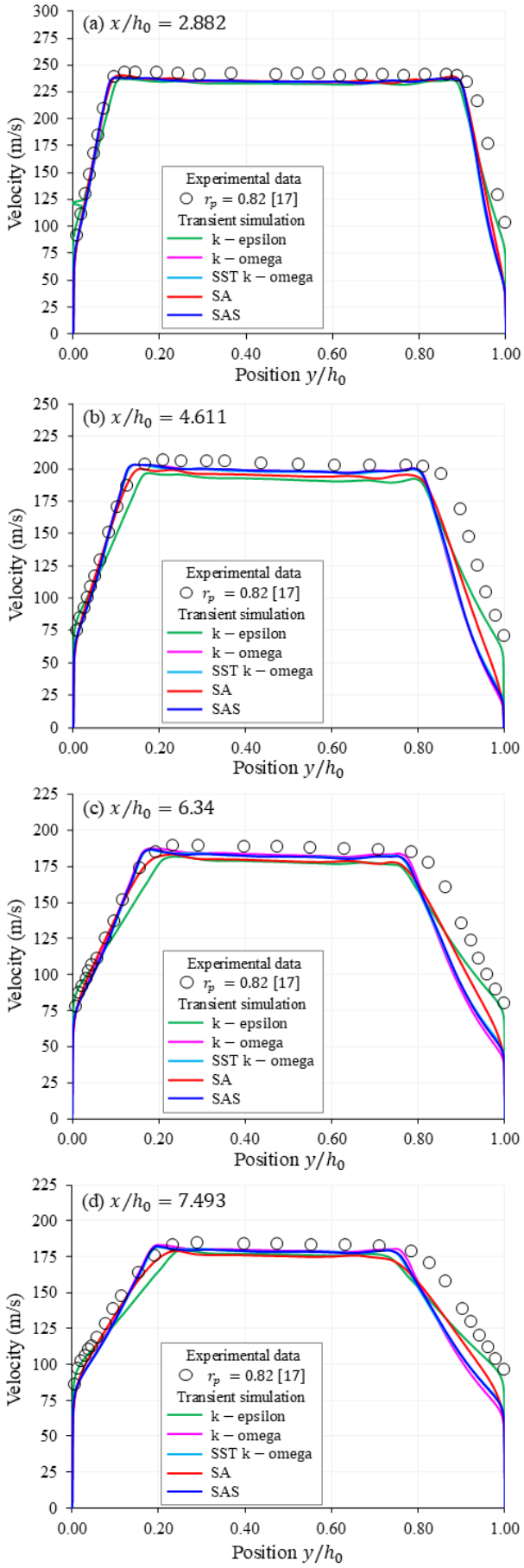


Figure 5. Comparison of curves from five turbulence models with experimental velocity data for r_p = 0.82 [17]

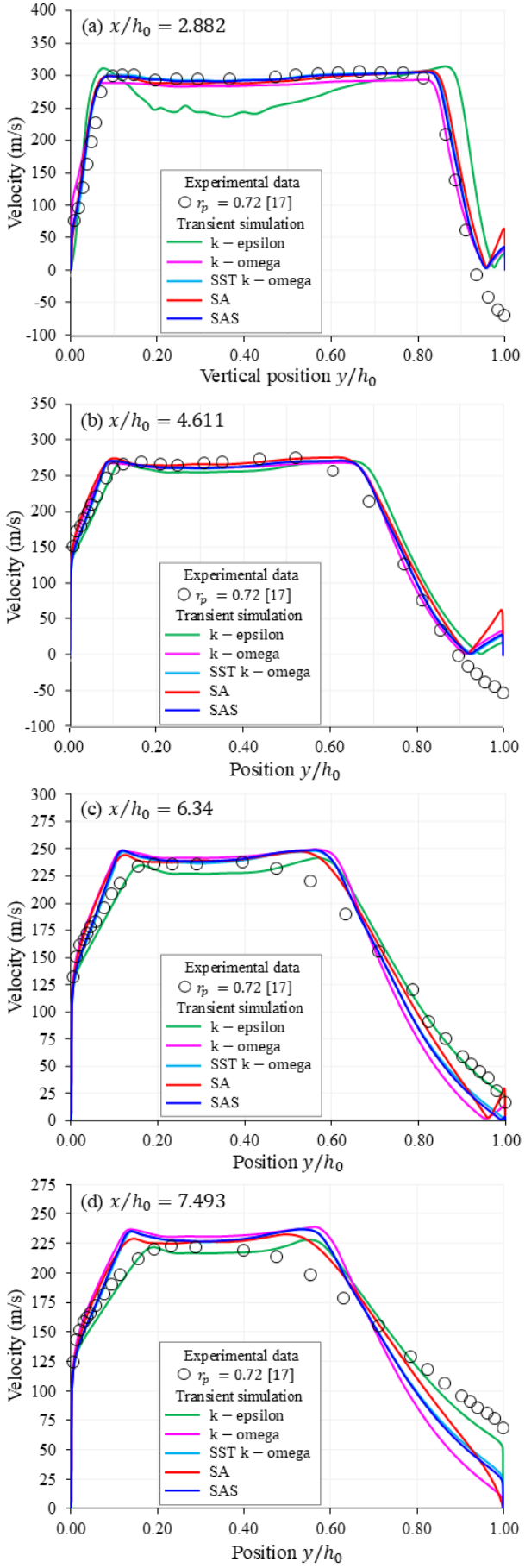


Figure 6. Comparison of curves from five turbulence models with experimental velocity data for r_p = 0.72 [17]

Backpressure causes velocity gradient changes, leading to opposite flow displacement and turbulent eddies near the upper diffuser wall, as shown by negative velocities at $x/h_0 = 2.882$ and $x/h_0 = 4.611$ in Fig. 6. The k-epsilon model exhibits anomalous behavior at this location compared to the other turbulence models, consistent with the pressure deviations noted in Fig. 4. Overall, significant deviations from experimental velocity profiles in the post-shock separation region highlight the urgent need for new or hybrid turbulence models to better capture these critical wall-adjacent flows.

3.3 Mach number field

The Mach number flow field evaluated for five turbulence models for $r_p = 0.82$ is illustrated in Fig. 7. Fig. 8 illustrates the behavior of the Mach number profiles along the diffuser from the inlet to the outlet, located at the position $y/h_0 = 0.5$.

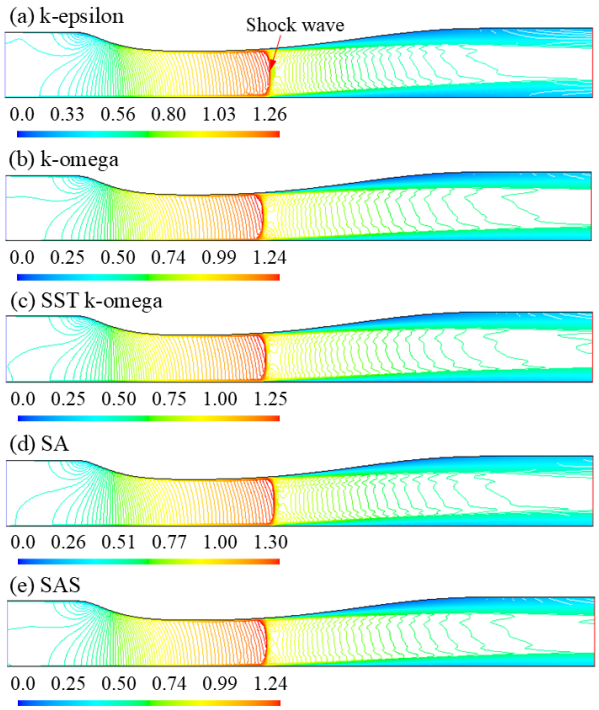


Figure 7. Differences in the behavior of the Mach number flow field for $r_p = 0.82$

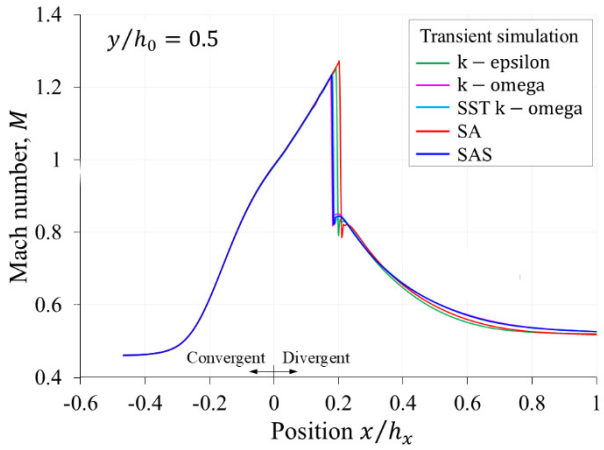


Figure 8. Mach number curves evaluated for five turbulence models for $r_p = 0.82$

The normal shock wave fronts from the computational simulations for $r_p = 0.82$ show slight discrepancies in their positions compared to the experimental data for Mach number $x/h_0 = 1.47$ ($x/h_0 = 0.169$) reported by Salmon et al. [31].

Table 6 presents the shock front positions, Mach numbers, and percentage relative errors with respect to the Mach number of 1.235 [31]. The farthest shock front position is presented for the SA turbulence model, which has a Mach number of 1.272 and shows a deviation with a percentage relative error of 2.995%. The smallest percentage relative error is presented for the SAS turbulence model, which has a Mach number of 1.233 with a percentage relative error of 0.162%.

Table 6. Mach number for $r_p = 0.82$ and percentage relative errors compared with experimental data

Model	x/h_x	Mach	Error %
k-epsilon	0.1919	1.252	1.376
k-omega	0.1765	1.226	0.728
SST k-omega	0.1816	1.239	0.323
SA	0.2022	1.272	2.995
SAS	0.1791	1.233	0.162
Salmon data [31]	0.169	1.235	-

Also shown are the Mach number flow field for $r_p = 0.72$, as illustrated in Fig. 9, and the Mach number profiles located at the position $y/h_0 = 0.5$, which are illustrated in Fig. 10.

It is observed that the shock front position for the k-epsilon turbulence model yields the highest relative error of 18.299% (Table 7), being further ahead and farther away from the experimental data for Mach number 1.353 at position $x/h_0 = 2.39$ ($x/h_0 = 0.276$) [31]. Meanwhile, the k-omega turbulence model exhibits a lag in the shock front, which has a percentage relative error of 8.178% for the Mach number.

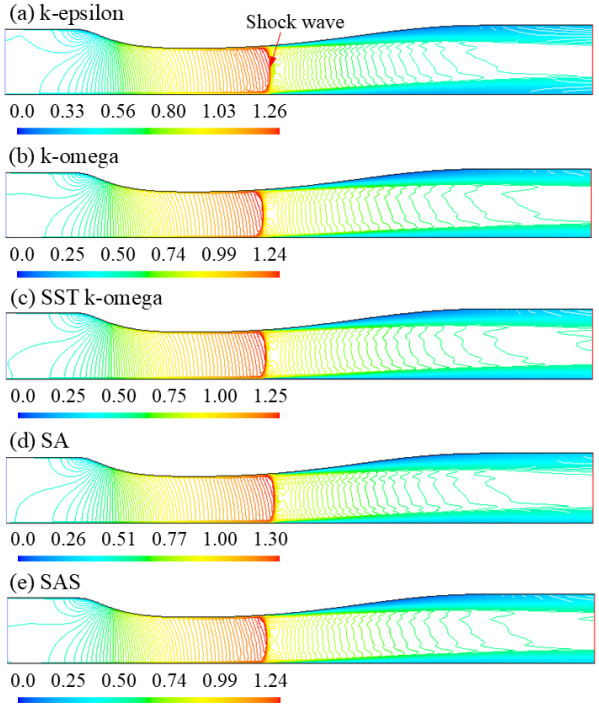


Figure 9. Differences in the behavior of the Mach number flow field for $r_p = 0.72$

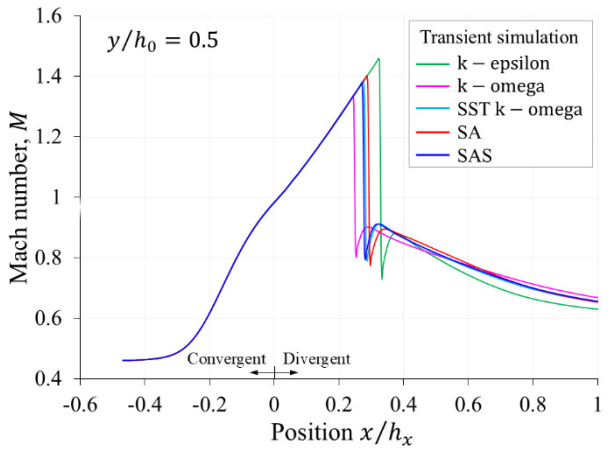


Figure 10. Mach number curves evaluated for five turbulence models for r_p = 0.72

It should be noted that, although the k-omega turbulence model presents the lowest percentage relative error for the Mach number compared to the other models (Table 7), this does not guarantee that its selection is correct, since its shock front position x/h_x = 0.2433 is lower than the experimental datum x/h_0 = 2.39 (x/h_x = 0.276) from Salmon et al. [31].

Meanwhile, the SAS turbulence model does present the best fit, since it has a position of x/h_x = 0.2716 and presents a percentage relative error of 11.821% for the Mach number. This Mach number comparison is consistent with the results presented previously regarding the overall average pressure difference of 2.62% (Table 5).

Table 7. Mach numberfor r_p = 0.72 and percentage relative errors compared with experimental data

Model	x/h_x	Mach	Error %
k-epsilon	0.3229	1.461	18.299
k-omega	0.2433	1.336	8.178
SST k-omega	0.2767	1.389	12.469
SA	0.2870	1.404	13.684
SAS	0.2716	1.381	11.821
Salmon data [31]	0.276	1.353	-

It is worth noting that other studies have reported validations of turbulence models, for example, considering turbulent flow in a 2D meshed domain with 6,561 elements reported by Georgiadis et al. [17] and a 2D meshed domain with 20,865 elements reported by Xiao and Tsai [41], whereas in the present work, 46970 elements were used in the 2D meshed domain. Meshed and refined domains in the regions adjacent to the walls help turbulence models achieve a better fit; however, due to their own design architecture, they do not always capture the flow phenomenon more accurately in the critical flow separation regions, and this is corroborated by the pressure, velocity, and Mach number results. Although the SAS turbulence model in transient state is the one that reports the best fit with respect to the experimental data reported in [17,30,31], compared to the other four turbulence models evaluated, the results obtained by SAS in the boundary layer separation and flow recirculation region must be taken into account.

The observed discrepancy between the numerical curves and the experimental velocity data highlights the intrinsic limitations of conventional RANS architectures for modeling massive shock-induced separation. Therefore, a fundamental research gap remains open, aimed at the design of new turbulence models that more accurately capture momentum transfer in transonic recirculation zones.

4. CONCLUSION

Based on the analysis carried out from the evaluation of five turbulence models: k-epsilon, k-omega, SST k-omega, SA, and SAS for transient turbulent flow in a 2D computational domain for pressure ratios r_p = 0.82 and $r_{p'}$ = 0.82, the following is concluded:

For the case of flow pressure on the transonic diffuser wall, when compared with experimental data, the comparative analysis demonstrates that the SAS provided the best overall agreement among the five turbulence models evaluated for the two pressure-ratio cases considered.

The five turbulence models fluctuate around the experimental velocity data in the central region of the flow; the SAS turbulence model is more closely fitted to the velocity data compared to the other four turbulence models evaluated. However, at the extremities of the shock front, in the flow separation region on the upper wall of the diffuser, the five turbulence models are far from the experimental velocity data.

The Mach number profiles evaluated along the transonic diffuser exhibit normal shock fronts. The profile of the SA turbulence model for r_p = 0.82 is far from the shock front, whereas for r_p = 0.72, the k-epsilon and k/hx-omega turbulence models are also far from the shock front. The SAS turbulence model is more closely fitted to the experimental Mach number data at the shock front.

However, despite the outstanding overall performance of the SAS model among the five models evaluated, this study reveals significant discrepancies in the prediction of the separation region induced by the shock wave–boundary layer interaction. This result confirms that this region remains one of the main challenges for conventional RANS models.

REFERENCES

[1] Wilcox, D.C.: *Turbulence modeling for CFD*, DCW Industries, La Cañada, California,3 ed., 2006

[2] Schlichting, H., Gersten, K.: *Boundary-layer theory*, Berlin Heidelberg, Germany, Springer Verlag, 9 ed., 2017

[3] Östlund, J., Muhammed-Klingmann, B.: Supersonic flow separation with application to rocket engine nozzles, ASME, Applied Mechanics Reviews, Vol. 58, No. 3, pp. 143–177, 2005

[4] Zmijanović, V. Rašuo, B., Chpoun, A.: Flow separation modes and side phenomena in an overexpanded nozzle, FME Transactions, Vol. 40, No. 3, pp. 111-118, 2012

[5] Ferziger, J.H., Perić, M., Street, R.L.: *Computational methods for fluid dynamics*, Springer, 4 ed., 2020

[6] Hunter, C.A..: Experimental investigation of separated nozzle flows, *Journal of Propulsion and Power*, Vol. 20, no. 3, pp. 527-532,2004

[7] Matsuo, S., Kanesaki, K., Nagao, J., Tawhidul, M. and Khan, I.: Effects of supersonic nozzle geometry on characteristics of shock wave structure, *Open Journal of Fluid Dynamics*, Vol. 2, no. 4A, pp. 181-186, 2012

[8] Génin, C. Stark, R., Haidin, O., Quering, K. and Frey, M.: Experimental and numerical study of dual bell nozzle flow, *Progress in Flight Physics*,Vol. 5, pp. 363-376,2013

[9] Wang, D., Wang, Z. and Chang, J.: Experimental study on dynamic characteristics of shock train in an isolator with different types of incident shocks, *Physics of Fluids*, Vol. 36, no. 7, 076108, 2024

[10] Allamaprabhu, Y., Raghunandan, B.N. and Moriñigo, J.A.: numerical prediction of nozzle flow separation: Issue of turbulence modeling, *Aerospace Science and Technology*, Vol. 50, pp. 31-43, 2026

[11] Tolentino, S.L.: Evaluation of turbulence models for the air flow in a planar nozzle, *Ingenius*, no. 22,pp. 25-37, 2019

[12] Haif, S., Kbab, H. and Benkhedda, A.: Altitude-compensating axisymmetric supersonic nozzle design and flow analysis, *INCAS Bulletin*, Vol. 15, no. 2, pp. 33-47, 2023

[13] Živković, S., Milinović, M. and Adamec, N.: Experimental and numerical research of a supersonic planar thrust vectoring nozzle via mechanical tabs, FME Transactions, Vol. 42, No. 3, pp. 205-211, 2014

[14] Liu, Y., Wu, J. and Lu, L.: Performance of turbulence models for transonic flow in a diffuser, *Modern Physics Letters B*, Vol. 30, no. 25, pp. 1650326-1-14, 2016

[15] Tolentino, S.L: Evaluation of turbulence models for the air flow in a transonic diffuser, *Revista Politécnica*, Vol. 45, no. 1, pp. 25-38, 2020 (In Spanish)

[16] Friedlander, D., Dudek, J.C. and Liou, M.F.: *Prediction of turbulent diffusing flows using FUN3D*, NASA/TM- 20220001759, pp. 1-24, 2022

[17] Georgiadis, N.J., Drummond, J.E. and Leonard, B.P.: *Evaluation of turbulence models in the PARC Code for transonic diffuser flows*, NASA TM-106391, January 1994

[18] Vujičić, M. and Crnojević, C.: Calculation of the turbulent flow in a plane diffuser by using the integral method, FME Transactions, Vol. 31, no. 2, pp. 69-74, 2003.

[19] Tolentino, S.L., González, O. and Mírez, J.: Comparative evaluation of DES and SAS turbulence models for incompressible flow in a Venturi tube, *INCAS Bulletin*, Vol. 12.no. 2, pp. 87-101, 2022

[20] Apte, D., Ge, M. and Coutier, O.: A comparative evaluation of turbulence models for simulation of unsteady cavitating flows, *Physics,flu-dyn,* pp. 1-42, 2023, arXiv:2303.08285v1

[21] Weiss, S., Mickan, B., Polanski, J., Oberleithner, K., Bär, M. and Schmelter, S.: Improved prediction of the flow in cylindrical critical flow Venturi nozzles using a transitional model, Vol. 113, pp. 363-389, 2024

[22] Tolentino, S.L., Mírez, J. and González, O.: Evaluation of turbulence models for incompressible flow in a Venturi tube, *FME Transactions*, Vol. 52, no. 4, pp. 534-543, 2024

[23] Tsukanov, R.: Comparison of various turbulence models for ejector nozzle CFD, *Aerospace Technic and Technology*, no. 1, pp. 4-17, 2026

[24] Segatori, C., Piano, A., Peiretti, B. and Millo, F.: Enhancing ducted fuel injection simulations: Assessment of RANS turbulence models using LES data, *SAE Technical paper*, 2024-01-2689, 2024

[25] He, Z., Guan, W., Wang, C., Guo, G., Zhang, L. and Gaviases, M.: Assessment of turbulence and cavitation models in prediction of vortex induced cavitating flow in fuel injector nozzles, *International Journal of Multiphase Flow*, 157, 104251, 2022

[26] Zhu, Z., Yang, H. and Chen, T.: Numerical study of turbulent heat and fluid flow in a straight square duct at higher Reynolds numbers, *International Journal of Heat and Mass Transfer*, Vol. 53, pp. 356-364, 2010

[27] Salehi, s., Raisee, M. and Cervantes, M.J.: Computation of developing turbulent flow through a straight asymmetric diffuser with moderate adverse pressure gradient, *Journal of Applied fluid Mechanics*, Vol. 10, no. 4, pp. 1029-1043, 2017

[28] Irbai, A., Siddiqui, O.,Kwiatkowski, T. and Shams, A.: Critical assessment of turbulence prediction in square duct flow, *Nuclear Engineering and Technology*, Vol. 58, no. 2, pp. 103937-1-16, 2026

[29] Kaya, M.N.: Shock-boundary layer interaction in transonic flows: Evaluation of grid resolution and turbulence modeling effects on numerical predictions, *Computer Modeling in Engineering & Sciences*, Vol. 145, no. 1, pp. 327-343, 2025

[30] Sajben, M. and Kroutil, J.C.: Effects of initial boundary-layer thickness on transonic diffuser flows, *AIAA Journal*, Vol. 19, no. 11, pp. 1386-1393, 1981

[31] Salmon, J.T., Bogar, T.J. and Sajben, M.: Laser doppler velocimeter measurements in unsteady, separated, transonic diffuser flow, *AIAA Journal*, Vol. 21, no. 12, pp. 1690-1697, 1983

[32] Bogar, T.J., Sajben, M. and Kroutil, J.C.: Characteristic frequencies of transonic diffuser flow oscillations, *AIAA Journal*, Vol. 21, no. 9, pp. 1232-1240, 1983

[33] Hosder, S. Grossman, B., Haftka, R.T., Mason, W.H. and Watson, L.T.: Quantitative relative comparison of CFD simulation uncertainties for a transonic diffuser problem, *Computers &Fluids*, Vol. 35, no. 10, pp. 1444-1458, 2006

[34] Launder, B.E. and Spalding, D.B.: *Lectures in mathematical models of turbulence*, A. P. London, New York, 1972

[35] Wilcox, D.C.: Reassessment of the scale-determining equation for advanced turbulence models, *AIAA Journal*, Vol. 26, no.11, pp. 1299-1310, 1988

[36] Menter, F.R.: Two equation eddy-viscosity turbulence models for engineering applications, *AIAA Journal*, Vol. 32, no. 8, pp. 1598-1605, 1994

[37] Spalart, P. and Allmaras, S.: A one-equation turbulence model for aerodynamic flows, *Technical Report AIAA-92-0439*, 1992

[38] Menter, F. and Egorov, Y.: The Scale-Adaptive Simulation method for unsteady turbulent flow predictions. Part 1: Theory and model description, *Flow, Turbulence and Combustion*,Vol. 85, pp. 113-138, 2010

[39] *Ansys Fluent theory guide, 2025*

[40] Sutherland, W.: The viscosity of gases and molecular force, *Philosophical Magazine series 5*, Vol. 36, no. 223, pp. 507-531, 1893

[41] Xiao, Q. and Tsai, H.M.: Computation of transonic diffuser flows by a lagged κ - ω turbulence model, *Journal of Propulsion and Power,* Vol. 19, no. 3, pp. 473-483, 2003

NOMENCLATURE

c_p	Specific heat at constant pressure
h_0	Throat height
γ	Specific heat ratio
k_t	Thermal conductivity
k_{eff}	Effective thermal conductivity
M	Mach number
P	Static pressure
P_o	Stagnation pressure
R	Gas constant
r_p	Pressure ratio
T_o	Stagnation temperature
t	Time
$\bar{\bar{\tau}}_{eff}$	Effective stress tensor
$\bar{\bar{\tau}}$	Stress tensor
u	Velocity
$\overline{u_i' u_j'}$	Reynolds stress term
x/h_x	Horizontal position
y/h_0	Vertical position
y^+	Dimensionless wall distance (y-plus)
ρ	Density

ACRONYMS

CFD	Computational Fluid Dynamics
DNS	Direct Numerical Simulation
DES	Detached-Eddy Simulation
FVM	Finite Volume Method
FSS	Free Shock Separation
LES	Large-Eddy Simulation
RANS	Reynolds-Averaged Navier-Stokes
RSS	RestrictedShock Separation

ЕВАЛУАЦИЈА МОДЕЛА ТУРБУЛЕНЦИЈЕ ЗА СТРУЈАЊЕ СА УДАРНИМ ТАЛАСИМА У ТРАНСЗВУЧНОМ ДИФУЗОРУ

С.Л. Толентино, Х. Мирес

У овом раду извршена је евалуација пет модела турбуленције (k-epsilon, k-omega, SST k-omega, SA и SAS) за случај турбулентног струјања у транс–звучном дифузору који се користи у експери–менталним испитивањима за генерисање ударних таласа. Модели су примењени у оквиру RANS приступа. Извршене су нестационарне симулације у дводимензионалним рачунским доменима за односе притисака rp = 0,82 и rp = 0,72, коришћењем софтвера ANSYS Fluent R16.2. За вискозност која зависи од температуре примењен је Сатерландов закон. Резултати су упоређени са експерименталним подацима за притисак, брзину и Махов број. Када је реч о притиску, SAS модел је дао глобалну средњу грешку од 2,62%. У зони одвајања струјања на горњем зиду дифузора (на крајевима фронта удар–ног таласа), свих пет модела је у одређеним областима показало значајна одступања од експери–менталних података за брзину. Што се тиче Маховог броја, модели су предвидели различите положаје фронта ударног таласа. За максимални Махов број на фронту ударног таласа, SAS модел је дао грешке од 0,162% (за rp = 0,82), односно 11,821% (за rp = 0,72).